

Environmental Effect on the Fluorescence Lifetime and Quantum Yield of Single Extended Luminescent Conjugated Polymers

Areifen Rassamesard,^{†,‡} Yi-Fang Huang,[†] Hsu-Yang Lee,[†] Tsong-Shin Lim,^{†,§}
Ming Chung Li,^{||,⊥} Jonathon David White,^{*,||} Jose Hector Hodak,^{*,‡,∇} Tanakorn Osotchan,^{‡,∇}
K. Y. Peng,[♦] S. A. Chen,[♦] Jui-Hung Hsu,[○] Michitoshi Hayashi,[#] and Wunshain Fann^{†,+,‡}

Institute of Atomic and Molecular Sciences, Academia Sinica, P.O. Box 23-166, Taipei 106, Taiwan, Department of Physics, Faculty of Science, Mahidol University, Rama 6 Rd., Bangkok 10400, Thailand, Department of Physics, Tunghai University, Taichung 407, Taiwan, Department of Chemistry, National Tsing Hua University, Hsinchu 30013, Taiwan, Molecular Science and Technology Program, Taiwan International Graduate Program, Academia Sinica, Taipei 115, Taiwan, Center for Condensed Matter Sciences, National Taiwan University, Taipei 106, Taiwan, Department of Photonics Engineering, Yuan Ze University, Taoyuan, Taiwan, ThEP Center, Commission of Higher Education, 328 Si Ayuthaya Rd, Bangkok 10400, Thailand, Department of Chemical Engineering, National Tsing Hua University, Hsinchu 300, Taiwan, Department of Materials and Optoelectronic Science, National Sun Yat-sen University, Kaohsiung, Taiwan, Institute of Polymer Science and Engineering, National Taiwan University, Taipei 106, Taiwan, Department of Physics, National Taiwan University, Taipei 106, Taiwan

Received: June 26, 2009; Revised Manuscript Received: September 4, 2009

To investigate the local environment's effect on the lifetime and quantum yield of extended polymer chains in the absence of intra- and interchain aggregation, short, rodlike polymers of poly(2,5-di-*n*-octyloxy-1,4-phenylenevinylene) (DO-PPV) were dissolved in chloroform and then embedded in a polystyrene matrix. The fluorescence lifetime was found to increase by 45% in moving from the solution to the matrix form. By using the absorption and emission spectra of the chloroform solution to estimate the radiative and nonradiative rate constants for the polymer in solution, along with calculations based on an exciton model, the corresponding decay rate constants for the polymer embedded in the matrix were obtained. The close agreement between the calculated and experimental values of fluorescent lifetime in the matrix proved the applicability of the exciton model used. On the basis of the model, the average quantum yield of isolated polymers in the matrix was calculated to be a factor of 2 higher than in solution—an effect arising from a 59% decrease in the nonradiative rate constant and, to a smaller extent, from a 20% increase in the radiative decay rate due to the different dielectric constants of the environments. These results suggest that by extending and isolating single luminescent polymers, high quantum yield devices are possible.

I. Introduction

Luminescent conjugated polymers have application as the active material in electroluminescent¹ and photovoltaic^{2,3} devices based on thin film technology. The performance of these devices is strongly affected by the polymer's electronic properties and photophysics. These in turn depend critically on steps taken in film preparation such as polymer concentration, dissolving medium (solvent), and thermal treatments.⁴ For example, in nonpolar solvents the extended chain conformation prevails, while in polar solvents individual polymers tend to coil up

tightly and multiple chain aggregates form.⁵ Because the molecular conformation adopted by the polymer in the film is correlated with that in solution, the solvent choice strongly affects the film's optoelectronic properties.^{6–8}

While the solution morphology influences film morphology, ensemble measurements have shown that the excited state lifetime of polymers differ significantly between the solution and film states. In thin films of CN-PPV⁹ and CN-ether-PPV,¹⁰ longer lifetime components have been observed in the film state which have been attributed to a longer radiative lifetime and to excimer emission.

Sartori et al. have shown that the conformation (i.e., extent of intramolecular aggregation) of single high molecular weight polymers is affected by the host medium.¹¹ Concentration-dependent time-resolved studies in poly(fluorene), poly(paraphenylene), and poly(4,40-diphenylenevinylene) have shown that the occurrence of these long-lived states with large Stokes shifts decreases by reducing the concentration of the polymer or by forming supramolecular threaded structures with cyclodextrins. This provides strong evidence that they indeed arise from interchain interactions.¹² In contrast, the fluorescence lifetime of PDHPT was observed to shorten when moving from

* Corresponding authors. E-mail: frjhh@mahidol.ac.th (J.H.H.) and whitejd@xiaotu.com (J.D.W.).

[†] Institute of Atomic and Molecular Sciences, Academia Sinica.

[‡] Mahidol University.

[§] Tunghai University.

^{||} Department of Chemistry, National Tsing Hua University.

[⊥] Molecular Science and Technology Program, Taiwan International Grad. Prog., Academia Sinica.

[#] Center for Condensed Matter Sciences, National Taiwan University.

[♦] Yuan Ze University.

[∇] ThEP Center.

[○] Department of Chemical Engineering, National Tsing Hua University.

[○] National Sun Yat-sen University.

⁺ Institute of Polymer Science and Engineering, National Taiwan University.

[‡] Department of Physics, National Taiwan University.

solution to thin films. This was interpreted as the result of interchain exciton migration and nonradiative decay at quenching sites.¹³

Clearly these interactions are dependent on material morphology on a nanometer scale, leading to a broad diversity of the properties of individual polymers.¹⁴ As this diversity is ensemble-averaged in traditional spectroscopy of bulk samples (films and solutions), it is important to study conjugated systems at the individual chain level in order to understand the fundamental photophysics and to compare the results to model predictions. Indeed, the extensive single molecule spectroscopy experiments performed on conjugated polymers,^{4–6,14–16} have provided a better understanding of the intermolecular interactions, showing that photoinduced processes also have a marked effect on the observed fluorescence lifetime. In studying the fluorescence decay dynamics of MEH-PPV dispersed in PMMA, Lin et al.¹⁴ found that abrupt intensity fluctuations are accompanied by simultaneous changes in the fluorescence lifetime. In short chains of MEH-PPV containing two or three emitting segments embedded in polystyrene, fluorescence lifetime was observed to increase after the first emitting segments bleach with a concomitant spectral blue shift.¹⁷

In order to better understand these results, it is necessary to develop a model of the conjugated polymer. The simplest model is one based on a distribution of segments of varying conjugation length brought about by distortions from the ideal planar-conjugated structure, cis-bonds, cross-links, and, tetrahedral defects.^{18,19} The absorption of light by these imperfect π -conjugated polymers leads to the formation of excited states that undergo a rapid relaxation with measured vibrational dephasing times of less than 1 ps²⁰ leading to the formation of singlet excitons. Diffusion of these excitons toward segments of the polymer that have lower π - π energy gaps then occurs faster than photon emission, causing a substantial Stokes shift contribution and emission spectra which are narrower than the absorption spectrum and not very sensitive to the excitation wavelength.¹⁰ In films or in solutions of conjugated polymers in poor solvents, this picture is complicated by the formation of excimers and interchain exciton delocalization, both of which lower the coupling to the ground state and increases the radiative lifetime.⁸ Excitons and excimers subsequently decay via radiative and nonradiative processes which determine the quantum efficiency of photoluminescence and ultimately the efficiency of the devices.²¹ Hence, knowing the magnitude of the various rates for deactivation is important to optimize their use as photoluminescent or as photovoltaic substrates.

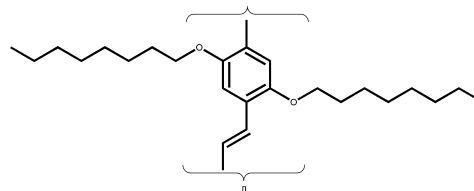
The work described here involves two main focuses. First, the static effect of the polymer microenvironment on extended DO-PPV chains in very dilute inert films (ca. $6 \times 10^{-3}\%$) and thus with minimized extent of intramolecular and intermolecular aggregation phenomena is investigated. Our work provides additional insight into previous studies that addressed fluorescence lifetime changes induced by a photophysical process¹⁷ or dealt with phenomena in neat films or moderate concentration (1–10%)^{6,9,22,23} of luminescent polymers in inert films.^{9,10} Our results show that on average the excited state lifetime of isolated polymers embedded in a polystyrene matrix increases by $\sim 45\%$ relative to that in a chloroform solution caused by a 36% reduction in the Huang–Rhys factor.

The second focus of this work is to test a model for estimating the nonradiative rates for polymers proposed by Lin et al.²⁴ and extended by Hayashi et al.²⁵ If this model is correct, it provides a basis with which to estimate the key parameters of fluorescence lifetime and quantum yield for isolated single polymers

embedded in an inert matrix based largely on parameters that can be easily measured in solution. Our calculations of the fluorescence lifetime, taking into account the effect of the dielectric constant of the medium on the nonradiative rate constant, agreed well with experimental results, confirming the essential validity of this exciton-based model for the prediction of nonradiative decay rates. On the basis of the decay rates, we obtain the experimentally difficult to measure fluorescence quantum yield for a very diluted polymer in an inert matrix.²² For the particular polymer/matrix combination used here, it was found to be a factor of 2 higher than in chloroform solution.

II. Experimental Section

A. Sample Preparation. DO-PPV [poly(2,5-dioctyloxy-*p*-phenylenevinylene); see below] was synthesized following a procedure similar to those of Sarnecki²⁶ and Askari²⁷ and fractionated using the method of Hsu et al.²⁵ The final sample had a molecular weight (M_n) of 7600 and polydispersity ($\delta = M_w/M_n$) of 2.1 as determined by gel permeation chromatography using polystyrene standards. This corresponds to a polymer of $\bar{n} = 30$ monomer units [determined by $(M_w/M_n)^{1/2}$] having a relatively narrow chain length distribution and contour length of ~ 15 nm. This contour length was comparable to the estimated persistence length of DO-PPV, indicating that these chains were predominately rodlike,¹⁹ ensuring that self-aggregation was unlikely to occur. A stock solution of the polymer was prepared in the good solvent chloroform (CHCl_3) to obtain a DO-PPV concentration of 10^{-6} M. For film studies, the stock solution was further diluted to 2×10^{-7} M and finally mixed in a 1:9 ratio with a chloroform solution containing 60 mg/mL of polystyrene ($M_w = 250$ kDa). The resulting DO-PPV molecular doping level in the final spin-coated films was approximately 1 DO-PPV polymer per 10^5 polystyrene molecules or $\sim 6 \times 10^{-3}\%$ w/w. The good solvent together with low concentration minimized multichain aggregates. During the sample preparation, contact with oxygen was minimized by purging all solutions with nitrogen and handling them in a nitrogen-filled glovebox. The films were spin-coated onto clean cover glasses that were then sealed in a nitrogen environment to slow down photodegradation of the film by oxygen.



B. Spectral Measurements. The solution absorption was measured in a 1 cm quartz cuvette using a GBC Cintra-20 instrument. The solution PL spectra was measured with the same cuvette using a Jobin Yvon FL3–22 spectrofluorometer in the front configuration geometry to minimize self-absorption. Excitation was at $\lambda_{\text{ex}} = 420$ nm. The solution photoluminescence spectra using a polymer concentration of 10^{-6} M or lower did not show any significant self-absorption distortions. Measurements in the polystyrene matrix were performed on isolated single DO-PPV polymers using a home-built confocal microscope system.¹⁹ Briefly, the output of an Ar ion laser ($\lambda_{\text{ex}} = 488$ nm) was directed to the epi-illumination port of an upright microscope (Nikon E600) by means of an optical fiber. A dichroic reflector (Chroma Technologies Z488) directed the beam toward the sample and through the microscope objective

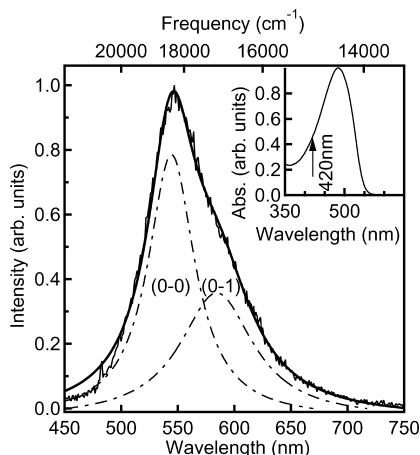


Figure 1. Photoluminescence (PL) spectra of dilute DO-PPV in CHCl_3 solution recorded at 10^{-7} mol/L (thin solid lines). The thick solid line is a fit to a sum of Lorentzians representing the 0–0 and the 0–1 transitions (dot-dashed lines). (Inset) Absorption spectrum with the excitation wavelength used for PL spectral measurements marked ($\lambda_{\text{ex}} = 420$ nm).

(Nikon CFI plan fluor100X, NA 1.3, oil immersion). The fluorescence was collected by the same objective, filtered with an interference filter (Chroma Technologies 515LP), and coupled into a multimode fiber that was also the confocal aperture. The fiber output was connected to a photon-counting detector and the sample was raster scanned with a piezoelectric stage (Physik Instrumente 517-3CL) to locate isolated DO-PPV polymers. Once found, the polymers were placed successively in the focal spot and interrogated. The PL spectrum was measured by directing the light through a monochromator (ACTON Research, sp-300) onto a liquid- N_2 -cooled charge-coupled device (CCD). All measurements were carried out at room temperature.

The fluorescence quantum yield for DO-PPV in solution was measured using standard techniques with MEH-PPV dissolved in chloroform as the standard.

C. Time-Resolved Measurements. DO-PPV in solution or matrix was excited at 460 nm (near the absorption peak, cf. Figure 1) with a 76 MHz repetition rate using the second harmonic of a titanium–sapphire mode-locked laser. Reversed time correlated single photon counting (TCSPC) was used for data acquisition.²⁸ The repetition rate and low start rate were chosen to minimize any possible pulse pileup effects on the fluorescence lifetime. The stop rate (76 MHz) was >1500 times higher than the start rate (typically <50 kHz in solution and <10 kHz for single molecule transients), ensuring minimal pulse pileup during the 12 ns time to amplitude converter window. As a result, for a 1.7 ns lifetime, the probability of detecting a photon from an excited state produced by the previous laser pulse was $p(t > 12\text{ ns}) \approx 9 \times 10^{-4}$.

For solution measurements, emission at 550 nm (near the emission peak, cf. Figure 1) was selected by directing light through a double monochromator (275DS, McPherson). A multichannel plate photomultiplier tube (MCP-PMT, R3809U-51, Hamamatsu), with a time resolution of 45 ps, was used for detection. The system incorporated a broad band preamplifier (6954B10, Philips Science), discriminator (model 9307, Ortec), and a time to amplitude converter (TAC; model 566, Ortec). A small fraction of the excitation pulse laser was sent to a fast photodiode to provide the stop signal that was detected by a constant fraction discriminator (TC455, Tenelec), delayed by a model 425A delay line (Ortec), and connected to the stop input for the TAC. Measurements in the polystyrene matrix were

performed using the same confocal system used for taking spectral data with an average excitation laser power of $1.1 \mu\text{W}$. Emissions were collected from 515 to 740 nm and directed to a Micro-Photon Devices (MPD) avalanche photodiode (time resolution ~ 45 ps) by means of a multimode optical fiber. A router was then used to split the electrical signal between a counting board (NI-PCI6602) and a time-correlated single photon counting (TCSPC) board (Becker & Hickl, SPC-600), allowing the fluorescence time trace (with 10 ms time resolution) and the fluorescence lifetime decay curve to be recorded simultaneously. This ensured that the emission signals originate from the individual molecules and allowed each single molecule signal to be corrected by its proper background.

Fluorescence lifetimes were obtained by fitting the experimental data to a model consisting of a single exponential function convoluted with the experimental instrument response function (IRF) using the commercial software FAST (Fluorescence Analysis Software Technology, ALANGO). Instrument response functions were obtained by recording the scattered light from a clean cover glass.

III. Results and Discussion

A. Photoluminescence Spectra. The photoluminescence and absorption spectra of DO-PPV in chloroform solution are shown in Figure 1. The absorption maximum at 484 nm ($20\,661 \text{ cm}^{-1}$) corresponds to the single chain species. The PL spectrum contained a prominent peak at $18\,367 \text{ cm}^{-1}$ and had a small shoulder at $17\,110 \text{ cm}^{-1}$. The former corresponds to the electronic 0–0 transition and the latter is the 0–1 vibronic transition for the extended chains.²⁹ To check for self-absorption effects, data were obtained at 10^{-5} , 10^{-6} , and 10^{-7} M concentrations of DO-PPV. While the spectrum at 10^{-5} M shows evidence of self-absorption for the 0–0 transition (Supporting Information), the data obtained at 10^{-6} and 10^{-7} M concentrations were not significantly affected by such distortion. The absorption and emission spectra in wavelength scale were fitted to a sum of two Lorentzian functions representing the 0–0 and 0–1 transitions. Superimposed on the emission spectrum in Figure 1 are Lorentzian fits to the two vibronic transitions for the data at the lowest concentration. The fact that the measured spectrum was well fit by a sum of these two spectra (dashed line in Figure 1) provided further evidence that aggregation is not present in the solution. This was further confirmed by aging the solution for 3 days, which resulted in no change in either the absorption or PL spectra.²⁹ The Huang–Rhys factor (S) constitutes a measurement of the changes in coordinates of the equilibrium position between the ground state and the excited state involved in the electronic transition. In the distorted harmonic potential approximation, the Huang–Rhys factor can be calculated from the ratio between the intensity of the 1–0 and 0–0 bands (see the Appendix for derivation). We thus calculated the Huang–Rhys factor from the fits by the ratio of the areas of these two vibronic bands. The use of the photoluminescence spectrum measured at 10^{-7} mol/L DO-PPV yielded $S = 0.75 \pm 0.01$, and an identical result was obtained from the data at 10^{-6} mol/L DO-PPV (cf. Supporting Information³⁰).

The ensemble PL spectrum in the polystyrene matrix obtained by summing the spectra of 37 single polymers is presented in Figure 2. Again the spectrum had a single prominent peak ($17\,549 \text{ cm}^{-1}$) and a smaller peak ($16\,125 \text{ cm}^{-1}$) corresponding to the 0–0 and 0–1 transitions, respectively. In single molecule experiments, the low concentrations involved ensure that there is no self-absorption-induced distortion to the emission spectra. Indeed, the summation of a large number of single molecule

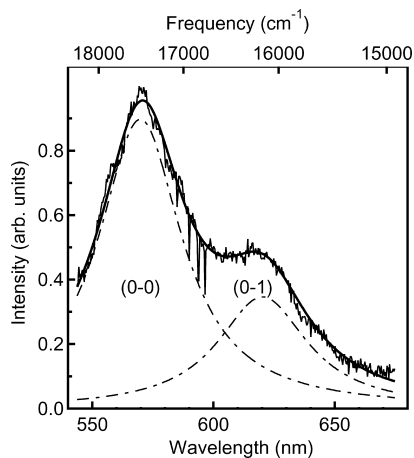


Figure 2. Summation of the PL spectra for 37 single chains of DO-PPV in polystyrene matrix. The experimental result is shown by the thin solid line. The thick solid line is the sum of two Lorentzians representing fits to the 0–0 and the 0–1 transitions (dot-dashed lines).

spectra yields an ensemble emission spectrum virtually free of self-absorption effects. As in solution, the measured spectra were well fit by a sum of two Lorentzians (lines in Figure 2), indicating that aggregation was also absent in the polystyrene matrix. In comparison with the solution spectrum, both the peak and shoulder positions were red-shifted by approximately 800 cm^{-1} and the Huang–Rhys factor ($S = 0.42 \pm 0.01$) was reduced by $\sim 44\%$. While the spectral red shift suggests that there has been an increase in the conjugation length of the emitting segments in the polymer, this is not unambiguous, as the different dielectric constants may also contribute to the shift. More unambiguous evidence for an increase in conjugation length is the change in the Huang–Rhys factor.²⁹ Previous experimental and theoretical work suggests that the Huang–Rhys factor decreases with increasing conjugation length in a conjugated polymer system,^{31–33} and experimentally it was found to decrease with temperature.⁷ The smaller value of S in polystyrene suggests that a more planar form of the polymer backbone exists in our films because this would result in an increase in the conjugation length. While in solution there is free torsional motion of the benzene ring along the polymer backbone, in a solid matrix the torsional motion is expected to be hindered after solvent evaporation is complete. In a good matrix, this lack of torsional motion should allow increased delocalization of the π -electrons along the polymer chain, resulting in increased conjugation length segments and a lowering of their energy gaps, assuming that the polymer is trapped in a conformation close to the ideal planar conjugated form.

B. Lifetime Measurements. The fluorescence lifetime decay curve of single polymers in solution is shown in Figure 3. The raw data (circles) were found to be a single exponential function, which is consistent with the existence of a single emissive species having an excited state lifetime (τ) of $0.69 \pm 0.03\text{ ns}$. The ensemble fluorescence lifetime decay curve of single polymers in the polystyrene matrix is shown in Figure 4. This curve was obtained by summing the individual fluorescence lifetime decay curves for 122 isolated polymers. The resulting fit was also a single exponential function and was well-fit using a lifetime (τ) of $1.07 \pm 0.02\text{ ns}$. In comparison to the lifetime in solution, polymers remained in the excited state $\sim 55\%$ longer when embedded in a matrix. This relative increase in lifetime has also been observed in thin films of CN-PPV⁹ and CN-ether-PPV.¹⁰

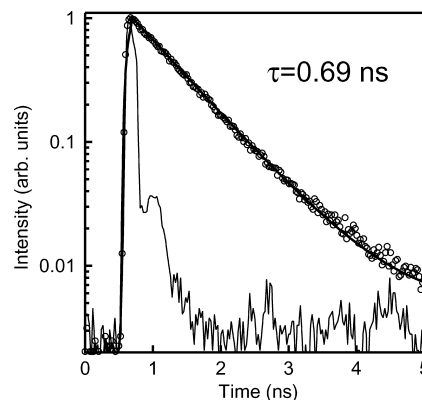


Figure 3. PL decay curve of DO-PPV in CHCl_3 solution. Excitation was at $\lambda_{\text{ex}} = 460\text{ nm}$ and detection at $\lambda_{\text{detect}} = 550\text{ nm}$. Experimental results are indicated by the open circles. The thick line is a least-squares fit to a single exponential function convoluted with the instrument response function of the MCP-PMT detector at 460 nm (thin solid line). The fluorescence lifetime for this solution is $\tau = 0.69 \pm 0.03\text{ ns}$.

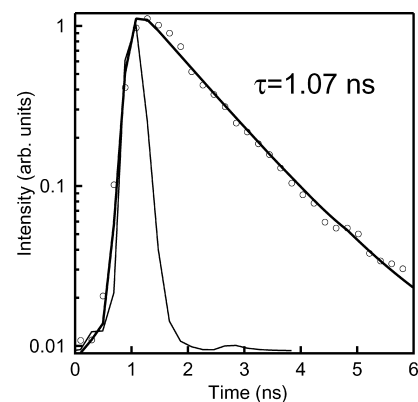


Figure 4. PL decay curve of DO-PPV dissolved in CHCl_3 and spin-cast into a polystyrene matrix ($\lambda_{\text{ex}} = 460\text{ nm}$, $515\text{ nm} < \lambda_{\text{detect}} < 740\text{ nm}$). The sum of the measured decay curves for 122 single chains is shown with open circles. The thick line is a least-squares fit to a single exponential function convoluted with the instrument response function for the (MPD) avalanche photodiode (thin solid line). $\tau = 1.07 \pm 0.02\text{ ns}$ in polystyrene.

The ensemble experiments provide only the population average value for the excited state lifetime. Single molecule experiments also allow for the observation of the behavior of individual classes of molecules, which is obscured in the ensemble data. Properties are expected to vary between individual polymers due to polydispersity (i.e., differences in chain lengths), the presence of defects, and the local environment resulting in a Gaussian distribution.¹⁷ Figure 5 presents the distribution of the excited state lifetimes for the 122 isolated polymers whose decay curves were summed in Figure 4. The distribution was fitted by a sum of two Gaussians (solid line) centered at $\tau_a = 0.96\text{ ns}$ with a full width of 0.36 ns and $\tau_b = 1.7\text{ ns}$ and a width of approximately 0.2 ns . The main component comprises 96%, while the small satellite mode constitutes 4% of the population. The fluorescence decay curves for polymers representative of each of the classes are shown in the inset of Figure 5. Both decays were clearly single exponential, indicating that within an individual polymer only one emitting species existed. The minor peak may be caused by polymers that have considerably shorter conjugation lengths.^{25,34} This shorter conjugation length could be the result of the relatively rare occurrence of more than one defect occurring in a single polymer that might allow it to fold back on itself. In previous work, it was estimated that up to 5% of these polymers contain such

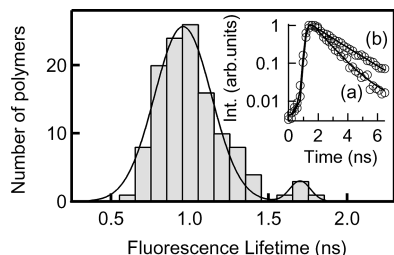


Figure 5. Fluorescence lifetime distribution of 122 single chains of DO-PPV in a polystyrene matrix. ($\lambda_{\text{ex}} = 460 \text{ nm}$, $515 \text{ nm} < \lambda_{\text{detect}} < 740 \text{ nm}$). The curve is a fit to a Gaussian function having $\tau = 0.96 \pm 0.18$ and $1.7 \pm 0.1 \text{ ns}$. The inset shows the PL decay curves of single polymers corresponding to the modes of the distribution. Experimental results are indicated by the open circles. The solid lines are fits that yielded the fluorescence lifetimes (τ) for these individual polymers: (a) 0.96 ± 0.02 and (b) $1.73 \pm 0.04 \text{ ns}$.

defects.¹⁹ One cannot, however, completely rule out the occurrence of other interchain interactions due to limited aggregation or segregation occurring during casting of the sample. Hence, some of the investigated objects may possibly have been small aggregates supporting excimers that are known to have lower radiative rates due to delocalization of the excited state wave function over multiple chains.^{8,12}

In the following discussion, we focus our attention on the 96% of polymers contained in the main peak. The wide variation in lifetime indicates that the microenvironment in which a polymer finds itself has a significant effect on its emission properties. This is not unique for short chain DO-PPV. For high molecular weight ($M_w \sim 200 \text{ kDa}$) MEH-PPV dissolved in toluene and dispersed in PMMA matrix, the fluorescence lifetime was found to be in the 0.4–1.2 ns range,¹⁴ while for low molecular weight ($M_w \sim 8 \text{ kDa}$) MEH-PPV dissolved in chloroform and embedded in polystyrene, the lifetime variation has been reported to be much smaller (1.2–1.4 ns).¹⁷ The mean and width of the lifetime distribution ($0.78 < \tau_a < 1.14$) for our $M_w \sim 16 \text{ kDa}$ DO-PPV thus lies between that observed for short and long chain MEH-PPV.

C. Calculation of Excited State Lifetime and Fluorescence Quantum Yield. In this section we present a calculation of fluorescence lifetime and decay rate constants of DO-PPV in the polystyrene matrix based on those in solution and on the molecular exciton theory as derived by Hayashi et al.²⁵ The fluorescence lifetime (τ) is related to the radiative (k_r) and nonradiative (k_{nr}) rate constants by the well-known equation

$$\frac{1}{\tau} = k_r + k_{\text{nr}} \quad (1)$$

In this equation, k_{nr} represents the sum of all nonradiative rates that compete with the fluorescence decay process. The fluorescence quantum yield (Φ) is given by

$$\Phi = \Phi^* \left(\frac{k_r}{k_r + k_{\text{nr}}} \right) \quad (2)$$

where Φ^* is the fraction of absorbed photons leading to the generation of singlet excitons. Generally for PPV-type polymers, $\Phi^* = 1$.³⁵ Substituting the measured fluorescence lifetime ($\tau = 0.69 \pm 0.03 \text{ ns}$) and the quantum yield ($\Phi = 0.32 \pm 0.02$) in the chloroform solution, one obtains $k_{r,\text{solution}} = 0.48 \pm 0.04 \text{ ns}^{-1}$ and $k_{\text{nr},\text{solution}} = 0.97 \pm 0.07 \text{ ns}^{-1}$ for DO-PPV in CHCl_3 .

The radiative rate for spontaneous emission from an excited molecule depends on the square of the refractive index (n) of the medium via the Strickler–Berg equation³⁶

$$k_r = n^2 \frac{8 \times 2303 \pi c \tilde{\nu}_{\text{ul}} \langle \tilde{\nu}_{\text{f}}^{-3} \rangle g_{\text{l}}}{N_{\text{Av}} g_{\text{u}}} \int \epsilon \, d(\ln \tilde{\nu}) \quad (3)$$

where $\tilde{\nu}$ is the frequency, $\tilde{\nu}_{\text{ul}}$ is the frequency of the transition, g_{u} and g_{l} are the degeneracies of the upper and lower states, N_{Av} is Avogadro's number, ϵ is the molar absorption coefficient, and c is the speed of light in a vacuum. The integral in eq 3 is over the entire electronic absorption band. By using the scaling of eq 3 with refractive index, we estimate the radiative decay constant for DO-PPV in the matrix based on that in solution to be

$$k_{r,\text{matrix}} = (n_{\text{polystyrene}}^2 / n_{\text{CHCl}_3}^2) k_{r,\text{solution}} = (1.60^2 / 1.45^2) k_{r,\text{solution}} = 0.58 \pm 0.05 \text{ ns}^{-1} \quad (4)$$

This is a $\sim 20\%$ increase over that in the solution and acts to decrease the fluorescence lifetime in the film. This is in contrast to the experimentally observed increase in lifetime, suggesting that the increase in the radiative rate constant must have been completely absorbed by a large decrease in the nonradiative rate.

The calculation of the nonradiative decay rates is more difficult, as these will not only be affected by index of refraction but also by the concentration of trap sites and quenchers that will differ between the solution and matrix. Hayashi et al.²⁵ proposed a model for the calculation of the nonradiative rate constant that is applicable to this system. The calculation is based on the molecular exciton theory²⁴ and on the assumption that only two vibronic transitions contribute to the spectra.²⁵ For internal conversion between an excited state b to ground state a [$k_{\text{nr}}(\text{b} \rightarrow \text{a})$], they obtained

$$k_{\text{nr}}(\text{b} \rightarrow \text{a}) = \left| \frac{V_s}{\hbar} \right|^2 \left(\sqrt{\frac{2\pi}{\omega_p(\omega_{\text{ba}} - \omega_p)}} \exp \left[-S - \left(\frac{\omega_{\text{ba}} - \omega_p}{\omega_p} \right) \times \left(\ln \left(\frac{\omega_{\text{ba}} - \omega_p}{S\omega_p} \right) - 1 \right) \right] \right)^2 I_s \quad (5)$$

where V_s is the coupling constant between states a and b, ω_{ba} is the average transition energy, ω_p is energy difference between the two vibronic bands, and S is the Huang–Rhys factor. While this equation is strictly valid only at $T = 0 \text{ K}$ (the nonradiative rate constant varies with temperature via its dependence on the Huang–Rhys factor), the use of eq 5 at higher temperatures has been shown to constitute a reasonable approximation.^{25,37} In this work, we use the average of the energies for the emission and the absorption maxima as an estimate for ω_{ba} , and the difference between the center positions of the peak and shoulder in the PL spectrum for ω_p .

From the absorption and emission spectra of DO-PPV in chloroform solution (Figure 1) one obtains $\omega_{\text{ba}} = 19\,514 \text{ cm}^{-1}$, $\omega_p = 1258 \text{ cm}^{-1}$ and $S = 0.75 \pm 0.01$. For the polymer embedded in the polystyrene matrix, the respective values are $\omega_{\text{ba}} = 19\,105 \text{ cm}^{-1}$, $\omega_p = 1425 \text{ cm}^{-1}$, and $S = 0.42 \pm 0.01$ (cf. Figure 2). As it is difficult to measure the absorption spectrum of single polymers, we have assumed that the absorption peak

TABLE 1: Comparison of Photophysical Parameters for DO-PPV in 10⁻⁷ mol/L Solution with Those Obtained for Molecules Embedded in the Inert Polystyrene Matrix

	CHCl ₃ solution	polystyrene matrix	difference
	experiment		
absorption peak/cm ⁻¹	20661 ± 2		
PL (0-0 peak)/cm ⁻¹	18367 ± 1	17549 ± 4	
PL (0-1 peak)/cm ⁻¹	17110 ± 3	16119 ± 8	
Huang-Rhys factor	0.75 ± 0.01	0.42 ± 0.01	-36%
lifetime/ns	0.69 ± 0.03	1.0 ± 0.02	+45%
quantum yield (Φ)	0.32 ± 0.02		
ω _p /cm ⁻¹	1258 ± 3	1425 ± 10	
ω _{ba} /cm ⁻¹	19466 ± 1	19115 ± 2	
refractive index (<i>n</i>)	1.45 ± 0.07	1.60 ± 0.08	+10%
	calculations		
k _r /ns ⁻¹	0.48 ± 0.04	0.58 ± 0.09	+21%
k _{nr} /ns ⁻¹	0.98 ± 0.07	0.5 ± 0.2	-48%
lifetime (τ)/ns		1.0 ± 0.3	
quantum yield (Φ)		0.6 ± 0.22	

was the same both in solution and in matrix form. These experimental values allowed I_s to be calculated for the medium embedding the polymers. Under the assumption that the coupling constant (V_s) is medium independent, we obtain the nonradiative rate constant in the matrix:

$$k_{nr,matrix} = \frac{I_{s,matrix}}{I_{s,solution}} k_{nr,solution} = 0.5 \pm 0.2 \text{ ns}^{-1} \quad (6)$$

In comparison, the nonradiative rate constant of the extended single chains in the polystyrene matrix was 48% lower than in solution. The main contribution to this difference arose from the difference in Huang-Rhys factors.

The fluorescence lifetime and quantum yield (Φ) and, hence, the light emission efficiency of the polymer in the matrix can be calculated from the decay rate constants. Making use of eq 1, we obtained the lifetime of DO-PPV in the matrix $\tau_{matrix} = 1.0 \pm 0.3$ ns. We note that this is in good agreement with our experimental value of 1.07 ± 0.02 ns (cf. Figure 4), confirming the applicability of the extended exciton model.^{24,25} From eq 2, the fluorescence quantum yield of the DO-PPV in polystyrene matrix is calculated to be 0.6 ± 0.2 , which represents an 88% increase of the luminescence efficiency in the polystyrene host relative to that in chloroform solution. All of the parameters and the key results for this work are summarized in Table 1. These results are consistent with the idea that exciton diffusion to a quenching site affects the excited state lifetime.¹⁰ In solution, the fluctuation of the bond angles imparts a dynamic component faster than the exciton lifetime and increases the diffusion length, which also increases the probability for excitons to visit quenching sites. Our interpretation is that the more rigid environment for polymers embedded in the polystyrene matrix constrained these fluctuations, which lead to a reduced exciton diffusion and quenching probability, thereby reducing the nonradiative rate.

Turning our attention to the range of observed lifetimes, we compare the variation with that predicted by the same theory. The presence of large torsion angles and other structural disorder in the polymer effectively breaks up the conjugation of the polymer into a number of segments with varying conjugation lengths.^{9,10,12,3,19,11,31} The conjugation length corresponds to the number of polymer repeating units over which the photogenerated exciton is delocalized. Exciton theory predicts that k_r for a

fully conjugated system of N units decreases with N .³¹ Thus, a variation in the average conjugation length of the emitting chromophores between individual polymers leads to a range of values of k_r and thus, by virtue of eq 1, results in a broadening of the distribution of excited state lifetimes. The radiative rate is given by³¹

$$k_r = D \frac{2A|\mu|^2}{N+1} \cot^2\left(\frac{\pi}{2N+2}\right) \quad (7)$$

where A is the Einstein coefficient for spontaneous emission, N is the number of repeating units in the chain, and D is a constant. It is straightforward to propagate a variation in N into one in k_r . The fluorescence lifetime is a function of both radiative and nonradiative rates (k_r and k_{nr}), which depend on the exciton delocalization length and possibly on the microenvironment of each polymer molecule. Thus, if σ_r/τ is the spread in the number of exciton delocalized units in the polymer, combining eqs 1 and 7 yields for the relative lifetime width σ_r/τ due solely to the variation in k_r

$$\sigma_r/\tau = \frac{\Phi_{polystyrene}}{(\bar{N}+1)} \left| \left| 1 - \frac{2\pi}{(\bar{N}+1)\sin\left(\frac{\pi}{\bar{N}+1}\right)} \right| \right| \sigma_N \quad (8)$$

where \bar{N} is the average number of exciton delocalized units in the polymer and $\Phi_{polystyrene}$ is the fluorescence quantum yield of DO-PPV in polystyrene. Experiments and time-dependent density functional calculations have established that the average conjugation length for π -conjugated polymers ranges from 4 to 7.^{31,38-41} We therefore use an average conjugation length $\bar{N} = 5$ with standard deviation $\sigma_N = 1.3$, which is consistent with results for a polymer with comparable molecular weight and polydispersity.³¹ Substituting these values, the previously calculated fluorescence quantum yield, and the measured fluorescence lifetime into eq 8, one obtains $\sigma_r = 0.13$ ns for the broadening contribution due to the variation of the radiative rates among emitting segments of the polymer. This accounts for about 77% of the experimentally measured width ($\sigma_r^{exp} = 0.18$ ns). Thus, it appears that microenvironment-induced variations in nonradiative decay rates contribute nearly 30% to the broadening of the distribution. This is consistent with the rather strong effect of the embedding matrix in our calculated nonradiative rate constant.

IV. Conclusions

The fluorescence lifetime and the fluorescence quantum yield of rodlike DO-PPV increased when this polymer was embedded in a polystyrene matrix, relative to that in a chloroform solution. The increase resulted from a combination of two factors. First, the ~48% reduction in the nonradiative rate caused by less efficient exciton quenching in polystyrene resulted in an increase in both lifetime and quantum yield. Second, the larger refractive index of polystyrene relative to that in chloroform caused a small increase (~20%) in the radiative rate, which also acted to increase quantum yield but which was not sufficient to compensate the effect of the decrease in the nonradiative rate on the fluorescence lifetime. Our measurements and calculations suggest that the media in which a polymer is embedded has a rather large contribution to the luminescence efficiency of the conjugated polymers. The close agreement between the mea-

sured and calculated lifetimes for the individual polymers in the matrix suggests that the exciton model of Lin et al.²⁴ as extended by Hayashi et al.²⁵ can be relied upon to estimate the fluorescence quantum yield of single molecules in a matrix when the quantum yield in the solution form is known. This provides a convenient guideline in the choice of polymer blends used for film fabrication. Finally, the factor of 2 increase in quantum yield for rodlike DO-PPV over the solution state suggests that, if long chain polymers can be isolated and extended, then one can expect an increase in quantum yield, allowing for highly efficient single molecule devices.

Acknowledgment. This work was supported financially by grants from the National Science Council Taiwan (ROC). A.R. and T.O. acknowledge financial support from the Thailand Research Fund through the Royal Golden Jubilee Ph.D. Program (Grant No. PHD/0194/2547). We regret that Prof. Wunshain Fann, who led this research project, did not live to see its publication. During his career he published over 100 original papers in the areas of free electron lasers, near-field optical microscopy, single molecule spectroscopy, and charge transport within conjugated polymer systems. His courageous personal battle against cancer over the past decade, coupled with his concern for the well-being of his graduate students, post-docs, and visiting researchers, along with his love of research, remains a model for those of us who had the privilege to know him and work under his leadership.

Supporting Information Available: Photoluminescence spectra of DO-PPV in chloroform at concentrations in the 10^{-5} – 10^{-7} mol/L range and a table with results of the calculations using the photoluminescence spectrum at 10^{-6} mol/L DO-PPV. This material is available free of charge via the Internet at <http://pubs.acs.org>.

Appendix

Let us consider the case in which the electronic transition from the electronically excited state b to the electronic ground state a takes place due to the emission of light. The electronic states a and b have vibration manifolds $\{v\}$ and $\{u\}$, respectively. We also assume that thermal equilibrium in the vibronic manifold of the electronic state b is achieved before the emission occurs. The emission intensity for this system can be expressed, under the Condon approximation and the Fermi golden rule, as

$$I(\omega, T) = k'\omega^3 \sum_{\{v\}} \sum_{\{u\}} P_{b\{u\}}(T) |\langle \Theta_{a\{u\}} | \vec{\mu}_{ab} | \Theta_{b\{v\}} \rangle|^2 \delta(\omega_{a\{u\},b\{v\}} + \omega) \quad (\text{A1})$$

where k' represents a constant, $P_{b\{u\}}(T)$ is the Boltzmann distribution function with temperature T , $\vec{\mu}_{ab}$ is the electronic transition dipole moment, $\hbar\omega_{a\{u\},b\{v\}} = E_{a\{u\}} - E_{b\{v\}}$ with, for example, $E_{a\{u\}}$ being the energy of vibronic manifold consisting of the electronic ground state and its vibrations, and $\hbar\omega$ is the photon energy.

Assuming displaced harmonic potential surfaces for the nuclear motions of the molecular system, eq A1 reduces to (for detailed derivation, please see refs 42, 43)

$$I(\omega, T) = k'\omega^3 |\vec{\mu}_{ab}|^2 \text{Re} \int_{-\infty}^{\infty} dt \exp[it(\omega_{ab} + \omega)] G_{ab}(t, T) \quad (\text{A2})$$

where

$$G_{ab}(t, T) = \prod_{\ell=1}^N G'_{ab}(t, T) \quad (\text{A3})$$

Here $G'_{ab}(t, T)$ can be given by

$$G'_{ab}(t, T) = \exp[S'_{ab}\{(\bar{n}_{\ell}(T) + 1)(e^{i\omega_{\ell}t} - 1) + \bar{n}_{\ell}(T)(e^{-i\omega_{\ell}t} - 1)\}] \quad (\text{A4})$$

where

$$\bar{n}_{\ell}(T) = (e^{\hbar\omega_{\ell}/kT} - 1)^{-1} \quad (\text{A5a})$$

and the Huang–Rhys factor is given by

$$S'_{ab} = \frac{\omega_{\ell}}{2\hbar} d'_{ab} \quad (\text{A5b})$$

with d'_{ab} being the displacement between the vibrational potential surface minimum of the electronic state a and that of b along the normal coordinate of the vibrational mode ℓ .

Note that eq A4 is the exact molecular formula for absorption within the Born–Oppenheimer approximation, Condon approximation, and displaced-harmonic potential approximation. Thus, if quantum chemistry (ab initio or density functional theory) methods can be applied to a given molecular system, one can predict absorption spectra of the molecular system.

For large systems, quantum chemistry methods may not be possible or practical. If the experimentally observed spectra of such systems exhibit a few peaks with broad widths, one can assume one high-frequency vibrational mode ($\hbar\omega_{\ell} \gg kT$) and one averaged low frequency mode ($\hbar\omega_{\ell} \ll kT$). In this case, one can see from eq A5a that $\bar{n}_{\ell}(T) = 0$ for the high-frequency vibrational mode so that eq A4 can reduce to

$$G'_{ab}(t, T) = \exp[S'_{ab}\{(\bar{n}_{\ell}(T) + 1)(e^{i\omega_{\ell}t} - 1) + \bar{n}_{\ell}(T)(e^{-i\omega_{\ell}t} - 1)\}] G_{ab}^H(t, T) = \exp[-S_{ab}^H + S_{ab}^H e^{i\omega_H t}] = \exp[-S_{ab}^H] \sum_{m=0}^{\infty} \frac{(S_{ab}^H)^m}{m!} \exp[im\omega_H] \quad (\text{A6})$$

The low-frequency vibrational modes lead to $\bar{n}_{\ell}(T) > 1$. In this case, one can apply the short time approximation to eq A5a, i.e.,

$$e^{\pm i\omega_{\ell}t} \approx 1 \pm i\omega_{\ell}t - \frac{(t\omega_{\ell})^2}{2} \quad (\text{A7})$$

Equation A4 reduces to

$$G_{ab}^L(t, T) = \exp\left[itS_{ab}^L\omega_L - S_{ab}^L\{2\bar{n}_L(T) + 1\}\frac{(t\omega_L)^2}{2}\right] \quad (\text{A8})$$

We finally obtain by substituting eqs A6 and A8 into eq A2

$$I(\omega, T) = k'\omega^3 |\vec{\mu}_{ab}^L|^2 \exp[-S_{ab}^H] \text{Re} \sum_{m=0}^{\infty} \frac{(S_{ab}^H)^m}{m!} \int_{-\infty}^{\infty} dt \times \exp \left[it(-\omega_{ba} + S_{ab}^L \omega_L + m\omega_H + \omega) - S_{ab}^L \{2\bar{n}_L(T) + 1\} \frac{(t\omega_L)^2}{2} \right] \quad (\text{A9})$$

The integral in eq A9 can be carried out analytically. It follows that

$$I(\omega, T) = A\omega |\vec{\mu}_{ab}^L|^2 \exp[-S_{ab}^H] \sqrt{\frac{\pi}{\{2\bar{n}_L(T) + 1\} \frac{S_{ab}^L (\omega_L)^2}{2}}} \times \sum_{m=0}^{\infty} I_m(\omega, T) \quad (\text{A10})$$

where

$$I_m(\omega, T) = \frac{(S_{ab}^H)^m}{m!} \exp \left[-\frac{(\omega_{ba} - S_{ab}^L \omega_L - m\omega_H - \omega)^2}{2\{2\bar{n}_L(T) + 1\} S_{ab}^L (\omega_L)^2} \right] \quad (\text{A11})$$

Equation A11 clearly shows that the vibronic progression is a function of the high-frequency mode with the weighting factor $(S_{ab}^H)^m/m!$. At each resonance, the intensity is given by

$$I_m^{\text{res}} \equiv I_m(\omega = \omega_{ba} - S_{ab}^L \omega_L - m\omega_H, T) = C \frac{(S_{ab}^H)^m}{m!} \quad (\text{A12})$$

with C being a constant so that the ratio of the $(m+1)$ th and m th vibronic peaks is given by

$$\frac{I_{m+1}^{\text{res}}}{I_m^{\text{res}}} = \frac{(S_{ab}^H)^{m+1}}{(m+1)!} / \frac{(S_{ab}^H)^m}{m!} = \frac{S_{ab}^H}{m+1} \quad (\text{A13})$$

Therefore, the ratio of the areas or intensities of the first and second peaks provide a reasonable estimate of Huang–Rhys factor S_{ab}^H . In our paper, we have used a Lorentzian function instead of a Gaussian function to estimate the ratio. The two line shape functions will provide the same S_{ab}^H value.

For the internal conversion (IC) rate constant, the same $G_{ab}(t, T)$ function is used under one high-frequency mode approximation. Using the saddle point method, one can obtain the rate constant shown in the paper. In calculations of the IC rate constant, the Huang–Rhys factor of a higher frequency mode (promoting mode) is important. This is due to the fact that the Franck–Condon factor is more preferable to achieve the energy conservation during internal conversion compared with that of the low-frequency vibrations.

References and Notes

- Friend, R. H.; Gymer, R. W.; Holmes, A. B.; Burroughes, J. H.; Marks, R. N.; Taliani, C.; Bradley, D. D. C.; Santos, D. A. D.; Bredas, J. L.; Logdlund, M.; Salaneck, W. R. *Nature* **1999**, *397*, 121.
- Chasteen, S. V.; Harter, J. O.; Rumbles, G.; Scott, J. C.; Nakazawa, Y.; Jones, M.; Horhold, H.-H.; Tillman, H.; Carter, S. A. *J. Appl. Phys.* **2006**, *99*, 033709.

- Yin, C.; Kietzke, T.; Neher, D.; Horhold, H.-H. *Appl. Phys. Lett.* **2007**, *90*, 092117.
- Schwartz, B. J. *Annu. Rev. Phys. Chem.* **2003**, *54*, 1419.
- Huser, T.; Yan, M. *J. Photochem. Photobiol. A* **2001**, *144*, 43.
- Müller, J. G.; Anni, M.; Scherf, U.; Lupton, J. M.; Feldmann, J. *Phys. Rev. B* **2004**, *70*, 035205.
- Quan, S.; Teng, F.; Xu, Z.; Zhang, T.; Qian, L.; Liu, D.; Hou, Y.; Wang, Y. *Mater. Lett.* **2006**, *60*, 1134.
- Nguyen, T.-Q.; Doan, V.; Schwartz, B. J. *J. Chem. Phys.* **1999**, *110*, 4068.
- Samuel, I. D. W.; Rumbles, G.; Collison, C. J. *Phys. Rev. B* **1995**, *52*, 11573.
- Chasteen, S. V.; Carter, S. A.; Rumbles, G. *J. Chem. Phys.* **2006**, *124*, 214704.
- Sartori, S. S. D. F.; Steven Hofkens, Johan; Van der Auweraer Frans, S. S. D. F. *Macromolecules* **2003**, *36*, 500.
- Petrozza, A.; Brovelli, S.; Michels, J. J.; Anderson, H. L.; Friend, R. H.; Silva, C.; Cacialli, F. *Adv. Mater.* **2008**, *20*, 3218–3223.
- Loi, M. A.; Gadermaier, C.; List, E. J. W.; Leising, G.; Graupner, W.; Bongiovanni, G.; Mura, A.; Pireaux, J.-J.; Kaeriyama, K. *Phys. Rev. B* **2000**, *61*, 1859LP.
- Lin, H.; Tabaei, S. R.; Thomsson, D.; Mirzov, O.; Larsson, P.-O.; Schelykin, I. G. *J. Am. Chem. Soc.* **2008**, *130*, 7042.
- Sun, W. Y.; Yang, S. C.; White, J. D.; Hsu, J. H.; Peng, K. Y.; Chen, S. A.; Fann, W. S. *Macromolecules* **2005**, *38*, 2966.
- Barbara, P. F.; Gesquiere, A. J.; Park, S. J.; Lee, Y. J. *Acc. Chem. Res.* **2005**, *38*, 602.
- Lim, T. S.; Hsiang, J. C.; White, J. D.; Hsu, J. H.; Fan, Y. L.; Lin, K. F.; Fann, W. S. *Phys. Rev. B* **2007**, *75*.
- Osterbacka, R.; Wohlgenannt, M.; Shkunov, M.; Chinn, D.; Vardeny, Z. V. *J. Chem. Phys.* **2003**, *118*, 8905.
- White, J. D.; Hsu, J. H.; Fann, W. S.; Yang, S. C.; Pern, G. Y.; Chen, S. A. *Chem. Phys. Lett.* **2001**, *338*, 263.
- Lanzani, G.; Cerullo, G.; Brabec, C.; Sariciftci, N. S. *Phys. Rev. Lett.* **2003**, *90*, 047402.
- O'Brien, D.; Bleyer, A.; Lidzey, D. G.; Bradley, D. D. C.; Tsutsui, T. *J. Appl. Phys.* **1997**, *82*, 2662.
- Heller, C. M.; Campbell, I. H.; Laurich, B. K.; Smith, D. L.; Bradley, D. D. C.; Burn, P. L.; Ferraris, J. P.; Müllen, K. *Phys. Rev. B* **1996**, *54*, 5516LP.
- Holzer, W.; Pichlmaier, M.; Penzkofer, A.; Bradley, D. D. C.; Blau, W. J. *Chem. Phys.* **1999**, *246*, 445.
- Lin, S. H.; Lee, S. T.; Yoon, Y. H.; Eyring, H. *Proc. Natl. Acad. Sci. U.S.A.* **1976**, *73*, 2533.
- Hsu, J. H.; Hayashi, M. T.; Lin, S. H.; Fann, W. S.; Rothberg, L. J.; Pern, G. Y.; Chen, S. A. *J. Phys. Chem. B* **2002**, *106*, 8582.
- Sarnecki, G. J.; Burn, P. L.; Kraft, A.; Friend, R. H.; Holmes, A. B. *Synth. Met.* **1993**, *55*, 914.
- Askari, S. H.; Rughooputh, S. D.; Wudl, F. *Synth. Met.* **1989**, *29*, 129.
- Kinoshita, S.; Ohta, H.; Kushida, T. *Rev. Sci. Instrum.* **1981**, *52*, 572.
- Huang, Y. F.; Shiu, Y. J.; Hsu, J. H.; Lin, S. H.; Su, A. C.; Peng, K. Y.; Chen, S. A.; Fann, W. S. *J. Phys. Chem. C* **2007**, *111*, 5533.
- See Supporting Information for results at 10^{-6} M.
- Chang, R.; Hsu, J. H.; Fann, W. S.; Liang, K. K.; Chang, C. H.; Hayashi, M.; Yu, J.; Lin, S. H.; Chang, E. C.; Chuang, K. R.; Chen, S. A. *Chem. Phys. Lett.* **2000**, *317*, 142.
- Cornil, J.; Beljonne, D.; Shuia, Z.; Hagler, T. W.; Campbell, I.; Bradley, D. D. C.; Brédas, J. L.; Spangler, C. W.; Müllen, K. *Chem. Phys. Lett.* **1995**, *247*, 425.
- Cornil, J.; Beljonne, D.; Heller, C. M.; Campbell, I. H.; Laurich, B. K.; Smith, D. L.; Bradley, D. D. C.; Müllen, K.; Brédas, J. L. *Chem. Phys. Lett.* **1997**, *278*, 139.
- Gierschner, J.; Cornil, J.; Egelhaaf, H. J. *Adv. Mater.* **2007**, *19*, 173.
- Samuel, I. D. W.; Rumbles, G.; Collison, C. J.; Friend, R. H.; Moratti, S. C.; Holmes, A. B. *Synth. Met.* **1997**, *84*, 497.
- Strickler, S. J.; Berg, R. A. *J. Chem. Phys.* **1962**, *37*, 814.
- Lin, S. H. *J. Chem. Phys.* **1973**, *59*, 4458.
- Graham, S. C.; Bradley, D. D. C.; Friend, R. H. *Synth. Met.* **1991**, *41*, 1277.
- Heun, S.; Mahrt, R. F.; Greiner, A.; Lemmer, U.; Bassler, H.; Halliday, D. A.; Bradley, D. D. C.; Burn, P. L.; Holmes, A. B. *J. Phys.: Condens. Matter* **1993**, *5*, 247.
- Tretiak, S.; Igumenshchev, K.; Chernyak, V. *Phys. Rev. B* **2005**, *71*, 033201.
- Wang, C. F.; White, J. D.; Lim, T. L.; Hsu, J. H.; Yang, S. C.; Fann, W. S.; Peng, K. Y.; Chen, S. A. *Phys. Rev. B* **2003**, *67*, 035202.
- Hayashi, M.; Yang, T. S.; Yu, J.; Mebel, A.; Lin, S. H. *J. Phys. Chem. A* **1997**, *101*, 4156.
- Shiu, Y. J.; Hayashi, M.; Mebel, A. M.; Chen, Y.-T.; Lin, S. H. *J. Chem. Phys.* **2001**, *115*, 4080.